

Detection of the Entropy of the Intergalactic Medium: Accretion Shocks in Clusters, Adiabatic Cores in Groups

Paolo Tozzi¹

Department of Physics and Astronomy, The Johns Hopkins University, Baltimore, MD 21218

Caleb Scharf

Space Telescope Science Institute, 3700 San Martin Drive, Baltimore, MD 21210

and

Colin Norman²

Department of Physics and Astronomy, The Johns Hopkins University, Baltimore, MD 21218.

ABSTRACT

The thermodynamics of the diffuse, X-ray emitting gas in clusters of galaxies is linked to the entropy level of the intra cluster medium. In particular, models that successfully reproduce the properties of local X-ray clusters and groups require the presence of a minimum value for the entropy in the center of X-ray halos. Such a minimum entropy is most likely generated by non-gravitational processes, in order to produce the observed break in self-similarity of the scaling relations of X-ray halos. Likely candidates are SNe heating, stellar winds, radiative processes, and nuclear activity. At present there is no consensus on the level, the source or the time evolution of this excess entropy.

In this framework a key question is whether the central entropy is the residual of the entropy originally present in the pre-collapse, intergalactic medium, or whether it is generated within the halos after collapse. Answering this question will allow a more precise determination of the energetic budget required to build an entropy floor, and lead towards an understanding of the nature of the sources of heating.

In this paper we describe a strategy to investigate the physics of the heating processes acting in groups and clusters. We show that the best way to extract information from the local data is the observation of the entropy profile at large radii in nearby X-ray halos ($z \simeq 0.1$), both at the upper and lower extremes of the cluster mass scale. The spatially and spectrally resolved observation of such X-ray halos provides information on the mechanism of the heating. We demonstrate how measurements of the size of constant entropy (adiabatic) cores in clusters and groups can directly constrain heating models, and the minimum entropy value.

¹Osservatorio Astronomico di Trieste, via Tiepolo 11, I-34131 Trieste, Italy

²Space Telescope Science Institute, 3700 San Martin Drive, Baltimore, MD 21210

We also consider two specific experiments: the detection of the shock fronts expected at the virial boundary of rich clusters, and the detection of the isentropic, low surface-brightness emission extending to radii larger than the virial ones in low mass clusters and groups. Both experiments are designed to measure the entropy in the low density gas far from the core, taking advantage of the large collecting power of the present X-ray telescopes (in this case XMM). Such observations will be a crucial probe of both the physics of clusters and the relationship of non-gravitational processes to the thermodynamics of the intergalactic medium.

Subject headings: galaxies: clusters: general – intergalactic medium – X-rays: galaxies

1. Introduction

The complex thermodynamic evolution of the hot, X-ray emitting, gas in clusters of galaxies is at the forefront of current efforts to understand these largest virialized systems. X-ray observations of cluster number counts, luminosity functions and temperature distributions indicate little apparent evolution in clusters back to redshifts as high as ~ 0.7 (e.g., Henry 1997, 2000; Rosati et al. 1998). These results provide one of the strongest challenges to high density cosmological models in which cluster evolution is expected to be occurring rapidly at low redshifts.

However, these tests are strongly dependent on the thermodynamic evolution of the intracluster medium (ICM, see Borgani et al. 1999 and references therein). In particular, the X-ray properties of X-ray halos depend on the entropy profile in the ICM. An ubiquitous minimum entropy, or entropy floor, in the external pre-infall gas, would break the self-similar behaviour of purely gravitational models, in agreement with the X-ray data. In terms of the global X-ray observables luminosity (L) and temperature (T), self-similar models predict $L \propto T^2$, while $L \propto T^\alpha$, with $\alpha \sim 3$, is observed (David et al. 1993, Mushotzky & Scharf 1997, Allen & Fabian 1998, Arnaud & Evrard 1998, Markevitch 1998), with evidence for a further steepening at group scales (Ponman et al. 1996; Helsdon & Ponman 2000, Xue & Wu 2000). Not only can the inclusion of an entropy minimum successfully reproduce the observed $L \propto T^3$ relationship, but it can also explain the flat density distribution observed in the cores of clusters and the low evolution of the L – T relation at high redshifts (see Tozzi & Norman 2000, hereafter TN). Recently an entropy floor has been detected in the core of groups (Ponman, Cannon & Navarro 1999, hereafter PCN; Lloyd–Davies, Ponman & Cannon 2000) providing direct evidence for this entropy excess in objects with temperatures between 1 and 3 keV. Evidence for a breaking of self-similarity also comes from the observation of a dramatic change in the chemical and spatial distribution properties of the gas at the scale of groups, below the observed temperature of 1 keV (Renzini 1997, 1999; Helsdon & Ponman 2000).

In hierarchical models of structure formation the local ICM is simply the high redshift IGM accreted into cluster and group scale potential wells. An examination of the equation of state of the IGM based on observations of the high redshift Ly α forest (Schaye et al. 1999; Ricotti, Gnedin & Shull 2000) yields an average entropy level which is at least an order of magnitude lower than that observed in the core of low temperature clusters, and that needed to explain the local properties of X-ray clusters and groups. Physical processes which could raise the entropy of the early IGM are SNe feedback, linked to the history of star formation, or radiative and mechanical processes driven by quasars (see Valageas & Silk 1999; Wu, Fabian & Nulsen 1999; Menci & Cavaliere 2000). It is, however, very difficult to model such processes *a priori*.

Our approach is instead to start from the properties of the ICM as observed in groups and clusters, and trace back the fundamental processes that drive the thermodynamic evolution of the gas. In order to simplify the possible scenarios, we consider two forms of entropy injection. First, the excess entropy may be interpreted as the fossil residual of an initial entropy floor imprinted in the external, pre-collapse IGM before the epoch of accretion. In this case, the heating occurs when

only the small, sub-galactic scales have collapsed, and the gas is heated at about the background density. Processes like starbursts can be very efficient in transporting large amount of energy out of the host galaxies (Strickland & Stevens 2000). In the second scenario, the entropy is the result of heating following the collapse of the baryons in group-sized potential wells ($M > 10^{13} M_{\odot}$). In this case the gas is heated at the average density reached in the virialized halos, which can be two orders of magnitude larger than the ambient density. These two scenarios imply a different energetic budget, since for a given entropy level, a larger energy per particle is required at higher densities. We hereafter refer to these two extreme situations as the *external* and *internal* heating cases, respectively.

In either scenario the enhanced gas density expected around actively accreting, massive clusters of galaxies (typically a factor of 10 with respect to the background value) could make it detectable in emission in the X-ray band even at distances larger than the shock radius, depending on its temperature and density. This gas has not yet been accreted or shocked, hence its entropy is indicative of the initial value present in the external IGM. The entropy level inside the shock radius will be much higher than the external level, as the result of strong shock heating driven by the accretion process. The entropy profile should then decrease towards the cluster center with a power law which results from the combination of shock heating and previous or ongoing non-gravitational heating.

At the low end of the mass scale, an external entropy floor gives rise to a flat, extended, low surface brightness emission, without any shocked accretion. In this case the gas has been accreted adiabatically, and the entropy remains at its initial value everywhere, even in the inner regions. With internal non-gravitational heating the profile can be more complex. Thus the investigation of lower luminosity, lower mass systems will be a useful complement to that of the accreting gas surrounding rich clusters.

There are therefore several potentially observable phenomena which allow us to probe the entropy histories of clusters: accretion shocks, external warm gas around clusters, highly extended isentropic emission in groups, and variations in the interior gas entropy profile for both clusters and groups. The combined observations of these features over a range of mass scales can test the internal versus external scenarios.

In the present work we investigate the predictions of the external and, to a lesser extent, the internal heating scenarios, and present observational strategies and feasibilities for studying their physical consequences. In §2 we discuss entropy based models and accretion processes for X-ray galaxy clusters. In the *external* heating scenario (§2.1) we demonstrate that the regions around rich clusters are particularly important. In the *internal* heating scenario (§2.2) the slope of the inner entropy profile can provide an indication of internal energy injection which followed the accretion. In §3 we present observational strategies to investigate the described scenarios. We consider the detection of accretion shock at the ICM/IGM interface; the expected properties of the accretion shock regions are described for a range of entropy levels in the external gas. We

then assess the feasibility of observing such accretion shock regions in real systems, using simulated XMM (see Dahlem et al. 1999) observations scaled to a nearby cluster (Abell 2029). We consider also strategies and feasibilities for observing groups, where an isentropic distribution of gas is expected. In §4 we briefly discuss stellar processes as a source of entropy, showing the impact of the proposed observations on the study of the nature of the heating sources. In §5 we present our conclusions.

2. Entropy-based models of X-ray clusters and groups

The evolution of the ICM is governed by both dynamics (and the underlying cosmology) and gas thermodynamics. A complete treatment of the physics of the gas necessarily includes shock heating and adiabatic compression (see the 1D models of Bertschinger 1985, Knight & Ponman 1997, Takizawa & Mineshige 1998, and the 3D numerical simulations of Evrard 1990, Roettiger et al. 1993, Metzler & Evrard 1994, Bryan & Norman 1998), and radiative cooling (see Lewis et al. 1999). An expanding accretion shock at the interface of the inner virialized gas with a cooler, adiabatically-compressed, external medium, located approximately at the virial radius of the cluster, is a longstanding prediction from such gravitationally-driven models. However, as discussed in the Introduction, gravitationally-driven models predict X-ray properties which scale self-similarly with mass and fail to reproduce X-ray observations of clusters.

The presence of a minimum entropy in the pre-collapse IGM has been advocated for some time as a way to naturally break the purely self-similar behaviour (Kaiser 1991, Evrard & Henry 1991). More recently, a minimum entropy has been detected (PCN) interior to clusters and all of its consequences have been re-visited. Models based on minimum entropy are able to explain the detailed shape of the L - T relation, predict its evolution, and help in explaining the cores and temperature profiles observed in clusters. In particular, we will use the model presented in TN that although having the limitation of being one-dimensional, does allow a semi-analytic treatment of shock heating, adiabatic compression and radiative cooling. With all of these processes being modulated by the cosmology and dark matter properties. The only free parameter in the model is, in the case of external heating, the initial entropy value. In the case of internal heating, the free parameter space is necessarily larger, depending on the epoch and distribution of the heating sources within the halo. Here we will limit the study of the internal scenario to a simple reference case, outlining only the most prominent features, without giving an exhaustive investigation of the many possible heating models.

In the following we describe the two scenarios, referring the reader to the work of TN and discuss in greater detail the resulting entropy profiles.

2.1. External heating

In the external heating scenario, a non-negligible initial entropy in the IGM introduces a mass scale where strong accretion shocks no longer form. Below this mass (at the scale of groups) is an effectively adiabatic regime, where gas is just compressed into the potential wells at constant entropy. The observed $L \propto T^3$ relationship is essentially produced by the resulting flattening of the density distribution in cluster cores, when shocks turn off completely (see Balogh, Babul & Patton 1999, Tozzi & Norman 1999 (TN)).

After the accretion, the entropy of each accreted shell of gas is kept constant, as long as the density is low and the cooling time (defined as $t_{cool} \propto \rho^{-1} T^{1/2}$ for $kT > 2$ keV) is correspondingly large. Cooling can be important in the central regions, depending also on the initial entropy level. Indeed, if the initial entropy is too low, cooling is the dominant process, leading to an excessive amount of cooled baryons. In this strong cooling regime (actually disfavoured by many observations and not considered further here), the semianalytical model breaks down. As stated above, further (internal) non-gravitational heating processes are not included in our external scenario.

The mass scale of shock formation is governed by the value of the IGM entropy $S \propto \log(K)$, where $K \equiv kT/\mu m_H \rho^{2/3}$ (here we assume that $\mu = 0.59$ for a primordial IGM). The value of $K = K_*$ that produces a good fit to the local L - T relation is $K_* = (0.2 \pm 0.1) \times 10^{34}$ erg cm² g^{-5/3} (see TN), which needs to be in place by at least the turn-around epoch for each shell. For a given entropy level, the temperature of the gas at the universal background density is derived as $kT \simeq 3.2 \times 10^{-2} K_{34} \times 10^{34} (1+z)^2$ keV (assuming the standard nucleosynthesis baryon density value). In terms of energetic budget, this value corresponds to a lower limit of $kT_{min} \simeq 0.1 (K_{34}/0.4)$ keV per particle in a Λ CDM universe ($kT_{min} \simeq 0.04 (K_{34}/0.4)$ keV in a tilted CDM with $\Omega_0 = 1$). Note that this value is within the energy budget expected from SNe heating (see Loewenstein 2000).

The observed entropy floor in the core of groups is about $K_{cl} \simeq 0.08 h^{-1/3} \times 10^{34}$ erg cm² g^{-5/3} (corresponding to $S \equiv kT/n_e^{2/3} \simeq 80 h^{-1/3}$ keV cm² using the definition of PCN, within an uncertainty of a factor of 2; see PCN, Lloyd-Davies, Ponman & Cannon 2000). We stress that in small mass halos, the central entropy excess is always expected to be smaller but close to the initial value at the epoch of accretion since the accretion proceeded adiabatically, and the cooling has been inhibited by the initial entropy level itself. Possibly, the observed value of K_{cl} may be different from that in the external IGM being accreted at $z = 0$ (the one we would want to detect) if substantial evolution in the entropy occurred since the accretion epoch. Indeed, since groups form typically at early lookback times, their central entropy could actually be lower than the present-day level in the external IGM if K_* grows with the cosmic epoch. We will consider this when discussing possible scenarios for actual observations.

Interestingly, the simplest assumption $K_* \geq K_{cl} = \text{constant}$ actually reproduces the observed break in scale invariance rather well. At low masses ($10^{13} - 10^{14} h^{-1} M_\odot$) the emitting gas will be very extended, without any discontinuity in the entropy since there are no shocks which would otherwise separate the accreting IGM from the accreted ICM. Indeed, data suggest that the total

luminosity of a group can vary by a factor of 2 or 3 after the inclusion of the undetected, low surface brightness emission extending up to the virial radius (see Helsdon & Ponman 2000). This is consistent with the prediction from the analytic model in TN, where, for a given temperature, the total luminosity (i.e., including the emission from all the gas within the shock radius) can exceed by a factor larger than 3 the luminosity included within $100h^{-1}$ kpc, a radius often used to define the luminosity of poor groups. As we will discuss in §3, detecting the missed emission from loose groups is one of the scientific aims of our proposed observational scheme.

Moving to higher mass scales, the initial entropy level has less effect on the outer cluster regions. The average entropy is dominated by the entropy produced in strong shocks. However, the initial entropy still contributes to building a central density core, even if the effect of cooling starts to be important in eroding the entropy plateau. An important point is that, in contrast to low mass systems, the gas density is still significant at radii larger than the virial radius. Specifically, at distances larger than the shock radius itself, the overdensity of the accreting gas will be $\simeq 10$ with respect to the background density. The entropy level of this gas is by definition the value K_* . We expect a considerable amount of such diffuse gas around massive halos. In particular, the most massive clusters are likely to be still accreting significant amounts of matter in most cosmologies, since they are the last objects to form in any hierarchical universe. The total accretion rate of matter for a cluster of 8 keV (roughly corresponding to a mass of $\simeq 10^{15} h^{-1} M_\odot$) is expected to be on average quite high at $z = 0$. The predicted average mass growth in baryons, computed in the extended PS framework (see, e.g., Lacey & Cole 1993), is about $f_b 0.24 \times 10^{15} M_\odot/\text{Gyr}$ for $\Omega_0 = 1$ with a tilted, cluster normalized CDM spectrum (tCDM) and $f_b 0.08 \times 10^{15} M_\odot/\text{Gyr}$ for $\Omega_0 = 0.3$ and $\Lambda = 0.7$ (Λ CDM). Here f_b is the universal baryonic fraction. In the following we will use the standard nucleosynthesis value $f_B = 0.02h^{-2}/\Omega_0$ for Λ CDM. This value gives similar baryonic accretion rates in Λ CDM and tCDM. However, we are forced to use a value at least two times larger in tCDM, in order to have the average baryonic fraction in halos as high as $\simeq 15\%$, as observed (White et al. 1993). As a general feature, the accretion rates are correspondingly higher at higher redshifts for the same masses. However, in this current work we will focus on $z \simeq 0$.

The break scale between adiabatic (low masses) and shock (large masses) regimes can be investigated by studying the dependence of the infall velocity v_i of the accreting IGM on the total mass of the system. Approximating the infall as an adiabatic flow, we calculate the infall velocity at the shock radius, where the gas is expected to be shocked and reach hydrostatic equilibrium. The effect of a constant entropy minimum K_* on the infalling IGM is to introduce a compression term proportional to the square of the sound speed $c_s^2 = \gamma K_* \rho_e^{2/3}$, where ρ_e is the external baryonic density and $\gamma = 5/3$ is the adiabatic index for a monoatomic gas. In fact, part of the gravitational energy goes into compression, to give for the infall velocity:

$$\frac{v_i^2}{2} = \frac{v_{ff}^2}{2} + \Delta W - \frac{c_s^2}{\gamma - 1} + \frac{c_s^2}{\gamma - 1} \left(\frac{\rho_{ta}}{\rho_e} \right)^{\gamma - 1}, \quad (1)$$

where v_{ff} is the free fall velocity, and ΔW is the contribution added to $v_{ff}^2/2$ to have the total work done by the gravitational potential (see TN). The fourth term on the right hand side results

from the initial condition $v_i = 0$ for a gas shell at the turnaround radius, when the gas had a density $\rho_{ta} \simeq \rho_{back}$. The compression term carries an increasing fraction of the total gravitational energy when the system mass is lower, or, since the sound speed is proportional to $K_*^{-1/2}$, when the entropy is higher.

The infall velocity can then be compared with the sound speed in the infalling gas, to test whether $v_i > c_s$ and shocks can develop. In Figure 1 the infall velocity computed at the shock radius is plotted as a function of the virialized mass, which is in turn a function of the redshift (here we have assumed an average mass growth for the dark halo commensurate with a Λ CDM universe). In the above picture only the external entropy level is needed to determine the transition between the adiabatic and the shock regime. The external density ρ_e , which determines the sound speed in the IGM, is obtained by imposing mass conservation at the accretion radius, plus the assumption that the accreted baryons are a constant fraction of the total virialized mass (see TN).

At early epochs, when the virialized mass is still low, the compression term is important and the infall velocity is lower than the sound speed. In this case, the accretion of the IGM proceeds entirely adiabatically, giving rise to an adiabatic core (insets Figure 1. As the virialized mass grows, the infall velocity eventually becomes larger than the sound speed, marking the epoch when shocks dominate (here we have neglected the small velocity of the shock front in the cluster rest frame). The infall velocity then asymptotically approaches the free fall velocity of the system. In Figure 1 an external constant entropy of $K_{34} = 0.3$ (where K_{34} is in units of $10^{34} \text{ erg g}^{-5/3} \text{ cm}^2$) has been assumed for a low density ($\Omega_0 = 0.3$) flat cosmology, for objects of mass $10^{14} h^{-1} M_\odot$ and $10^{15} h^{-1} M_\odot$. At lower masses, the transition from the adiabatic to the shock regime occurs later, giving rise to a relatively larger adiabatic core. From Figure 1 we can also see that for low mass systems ($M < 10^{14} M_\odot$), a growing fraction of the accreted baryons retains the pre-collapse entropy level. This fraction approaches unity at the scale of poor systems and groups, providing self-consistency with our expectations of isentropic gas in groups. Note that the transition between the adiabatic and the shock regime is marked by a transition radius r_t within which an approximately constant baryonic mass is contained. This can provide a meaningful observable as further discussed in §3.

As a consequence of the above picture, the entropy profiles change dramatically along the mass sequence: flat in low mass halos, steep and discontinuous for large masses. The steep part of the profile corresponds to strongly shocked gas, while the flat part is the adiabatically accreted gas. External to the shock, the accreting gas is simply adiabatically compressed. In the following sections we will describe in greater detail the resulting entropy profiles.

2.2. The entropy profile with external heating

We focus first on large mass scales, where a strong accretion shock is expected irrespective of the initial entropy level. Such an accretion shock is likely to occur at approximately the virial

radius, where the gas density can typically be a factor $\simeq 1000$ lower with respect to that at the cluster center. A simple relation exists between the density jump and the temperatures of the hot internal, and colder external, gas (Landau & Lifshitz 1959, see Cavaliere, Menci & Tozzi 1997, 1999):

$$\rho_i/\rho_e = 2\left(1 - T_e/T_i\right) + \sqrt{4\left(1 - T_e/T_i\right)^2 + T_e/T_i}, \quad (2)$$

where ρ_i and T_i are the internal gas density and temperature. The external density ρ_e and temperature T_e refer to the infalling gas just prior to being shocked. Note that T_e is *not* simply the temperature of the field IGM. The accreted IGM will experience adiabatic compression prior to reaching the accretion shock, thus $T_e = \mu m_p K_* \rho_e^{2/3}$. The overdensity of the baryons with respect to the background value is expected to be $\simeq 10$ for rich clusters both in Λ CDM and in tCDM. This would correspond to temperatures of $kT_e \simeq 3.2 \times 10^{-2} K_{34} \delta^{2/3} \simeq 0.15 K_{34}$ keV at $z = 0$. However, since in tCDM we are forced to assume a baryonic density larger than a factor of 2 (with respect to the standard nucleosynthesis value), the external temperature T_e for a given K_* and δ will be about 60 % larger.

To compute the internal density at the shock boundary, we could use the detailed and self-consistent density and temperature profile of the ICM resulting from a minimum entropy model, as derived in TN. However, the density profiles can be fitted to a good approximation with a β model (Cavaliere & Fusco Femiano 1976), at least at large radii where the cooling time is large, as it is shown in Figure 2. Therefore for simplicity we use it to approximate the gas density internal to the shock:

$$\rho = \rho_c \left(1 + (r/r_c)^2\right)^{-\frac{3}{2}\beta}, \quad (3)$$

where r_c is the core radius. For a flat temperature profile, the observed X-ray surface brightness at the shock radius r_s can be written as:

$$\Sigma = \Sigma_c \left(1 + (r_s/r_c)^2\right)^{-3\beta+1/2}. \quad (4)$$

In this case a simple inversion from surface brightness to density within the shock radius is given by:

$$\frac{\rho}{\rho_c} = \left(\frac{\Sigma}{\Sigma_c}\right)^{1/(2-1/3\beta)}. \quad (5)$$

For a β model, the discontinuity in the surface brightness expected at the shock is approximately $(\rho_i/\rho_e)^{2-1/3\beta} (T_i/T_e)^{1/2}$ (for $T_e \geq 1$ keV) with respect to the extension of the pure beta model to the shock radius. In the case in which there is no shock ($\rho_i/\rho_e = 1$) and the temperature profile decreases adiabatically as $T \propto \rho^{2/3}$ (expected in small groups), we can use the same functional form, replacing β with an effective β' which accounts for the mild dependence of the emissivity ϵ on temperature. In the case of pure bremsstrahlung and temperature $kT > 2$ keV, $\epsilon \propto T^{1/2}$ and $\beta' = \frac{7}{6}\beta$ (see Ettori 1999). At lower temperatures we must include the contribution from line emission, which is significant in the wide energy band of XMM (0.1 – 12 keV). For $0.1 < kT < 2$,

$\epsilon \propto \text{constant}$ with good approximation if the metallicity is about one third solar, virtually removing the temperature dependence and giving $\beta' = \beta$ again. The entropy jump can therefore be detected when both the X-ray surface brightness (from which density is determined) and the temperature are measured at the shock radius. In Figure 2 the surface brightness and the emission weighted temperature profiles are shown for three relevant cases of the external scenario, the same that will be discussed in detail in §3.

The effect of the accretion shocks is to raise the entropy over its initial (external) level. Since the transition from the adiabatic accretion to the shocked accretion is very fast (with the shock radius rapidly approaching the virial one, see Figure 4, third panel), the transition between the two regimes is recorded in the entropy profile as a sudden change of slope at the transition radius r_t . In the inner part the adiabatic core is visible (though eventually it will be partially erased by cooling), while in the outer, shocked regions a featureless power law profile is expected. A reference slope for this power law can be derived to a first approximation with the usual assumption of an isothermal profile: $\rho \propto r^{-2}$ gives $K \propto r^{4/3}$. This value is close to the $K \propto r^{1.1}$ predicted from the model (see TN), where a temperature gradient is present due to further adiabatic compression after accretion, and the density distribution is somewhat steeper than -2 . In other words, the gas in cluster is well described by a polytropic distribution with a polytropic index $\gamma_p \simeq 1.2$ (see Loewenstein 2000; TN). The expected entropy profiles in the external heating scenario are shown in Figure 3 for two objects of $M = 10^{15} H^{-1} M_\odot$ and $M = 10^{14} H^{-1} M_\odot$. We can see the entropy core partially erased by cooling within $r < 0.1 R_{vir}$, and the shocked gas with the characteristic slope $K \propto r^{1.1}$ at $r \simeq 0.1 - 0.3 h^{-1}$ Mpc.

2.3. Internal heating

How do these predictions change in the internal heating scenario? A first major difference is that the gas is heated when it is at much higher densities, and the change of entropy for a given energy input is consequently lower. In other words, to reproduce the breaking of the scale invariance in X-ray halos, a larger energy budget is needed in the internal scenario with respect to the external one. In the internal heating case, the IGM is essentially cold when it is accreted, and the gas always experiences strong shocks, even in low mass objects. In this case, the gas may be detected via emission in the UV band (and may be related to the UV excess detected around nearby clusters, see Lieu, Bonamente & Mittaz 2000). Alternatively, such gas may be seen in absorption against bright background sources, in the X-ray band if $kT \simeq 0.1$ keV (see Hellstein, Gnedin & Miralda-Escudé 1998), or in the UV band if $kT \simeq 0.01$ keV. In the last case OVI, which peaks at $\simeq 0.03$ keV in collisional equilibrium, is the best diagnostic (K. Sembach, private communication).

It is worth recalling that in the absence of any heating, in the central regions of halos the entropy gained by shock heating alone is not enough to prevent the gas from cooling. In fact, the absence of an initial extra entropy would result in a cooling catastrophe (see White & Rees 1978, Blanchard, Vall Gabaud & Mamon 1996). Furthermore, the combination of shock heating and

central cooling (without additional heating) is, in fact, not able to generate an entropy floor by the selective removal of the lowest entropy gas in the very center (see TN), a mechanism sometimes advocated to explain the entropy plateau (see PCN).

In the internal heating scenario, the number of free parameters is larger than one and dependent on the model used to describe the heating sources. Here we assume a simple phenomenological model, with a distribution of sources of equal mass (or output) given by a King profile with a large core (about 1/2 of the virial radius). The number of the heating sources is then normalized to the total mass of the given halo. The absolute number density of the sources is clearly degenerate with the average heating rate associated with each source, since only the global heating (as a function of the radius r) is relevant to the final entropy profile. Therefore, for each heating model we quote only the average heating per particle released up to the present epoch. Note that the heating is defined as the amount of energy dumped into the ICM, which can clearly be different from the total energy budget of the sources, depending on the gas heating efficiency.

We note that the difference in the energy budget between the internal and the external heating, is further exacerbated by cooling. Indeed, if the internal heating is not rapid enough to keep the density low and prevent further cooling, the densities in cluster centers will be always very large, and the same final entropy profile will require a very large energy budget. A direct consequence is that if the heating is not large enough, the energy input will be rapidly re-emitted by the high density gas, no matter how much energy has been released (see, e.g., Lewis et al. 1999).

The heating rate must have a dependence on z ; indeed, if the heating starts in the halo but at very early epochs, before a non-negligible amount of mass of the final halos has been accreted, the gas never reaches high overdensities and the properties of the external scenario are reproduced. Here we assume (motivated by the need to reproduce the observed L - T relation) that the heating rate peaks at $z \simeq 1$, with an exponential decline at higher redshifts, and a mild power law decline $\propto (1+z)^2$ for $z < 1$. The final energy budget is, in this case, mass dependent, since the number of sources is larger in higher mass halos. Moreover, enhanced heating is expected in the center, where the density of the heating sources is higher.

For the assumed peak redshift $z = 1$, we calibrate the energy budget by requiring consistency with local properties (e.g., fitting the L - T relation). We find that a total budget of about 1 – 2 keV per particle in clusters ($M = 10^{15} h^{-1} M_{\odot}$) and 0.5 – 1 keV in small clusters ($M = 10^{14} h^{-1} M_{\odot}$) can reproduce approximately the scaling relation for X-ray halos (see also Figure 4). Despite the uncertainties in the internal heating model, we always find that the energetic budget is more than an order of magnitude larger with respect to the external scenario in order to reproduce approximately the L - T relation. This estimate is robust and it is expected also on the basis of a simple analytical calculation, since the typical overdensities within virialized halos are of the order of few hundred, while the typical overdensities in the external accreting gas are $\delta \leq 10$ (see TN). The energetic budget in the internal scenario may be too high to be provided by SNe heating only. In this perspective, the comparison of the external and internal scenario may put constraint on the

nature of the heating sources.

In Figure 3 we show the resulting entropy profiles, in comparison to those of the external scenario. In a massive halo, the relatively flat distribution of heating sources results in a flatter entropy profile in the center $K \propto r^{0.5}$, while in the external regions the same profile of the external case $K \propto r^{1.1}$ is recovered. The slope of the inner profile depend on the total amount of energy injected, as shown by the labels in Figure 3. The same amount of heating in a smaller halo ($M \simeq 10^{14}h^{-1}M_{\odot}$) results in a larger entropy core that emerges in the central regions. In the regions where a negative entropy gradient developes, we expect instabilities and mixing. We do not show the case of very small halos, since large negative entropy gradients develop with consequent instabilities that cannot be included in the present treatment. The effect may be real, in the sense that in small halos the effect of the internal heating may disrupt the profile resulting from adiabatic/shocked accretion, and can eject virtually all the gas from the potential well, giving a patchy and irregular surface brightness. This possibility should be investigated with fully 3D numerical simulations.

In principle, measuring the entropy profile at a radius $\simeq 0.1R_{vir}$ in high and medium mass halos, can reveal a signature of the internal heating scenario as a departure from the profile expected in the external scenario. However, we emphasise that this is just an example based on a particular choice of the internal heating distribution, and in some cases the internal heating may result in an entropy profile very similar to that of the external scenario. A more comprehensive investigation of the parameter space in the case of internal heating will be presented in a future work.

It is worth noting, nevertheless, that observations at a radius $r \simeq 0.1R_{vir}$ will be less difficult with respect to those at the shock radius, due to the higher surface brightness. The signal will be much higher and the entropy profile can be reconstructed in greater detail (see PCN). In principle, it will also be possible to produce entropy maps inside clusters. In the assumption that the ICM has not been stirred due to massive merger events (an assumption which is implicit for the spherical model used here and described in TN), the entropy maps would trace the patches of major heating internal to the cluster.

In Figure 4 we show the time evolution of a cluster, a small cluster and a group in a Λ CDM cosmology for the internal (dashed lines) and external heating (continuous line) scenarios. The external scenario assumes $K_{34} = 0.3$, while the internal scenario assumes an energy budget of $\simeq 0.9$ keV per particle. The lowest mass ($M = 10^{13}h^{-1}M_{\odot}$) is not shown for the latter model. At $z = 0$ the total luminosities and the emission weighted temperatures are quite similar, and it is not possible to distinguish the two scenarios from the statistical properties of the X-ray halo population only; both scenarios fit the $L-T$ relation (as can be confirmed from the final luminosities and temperature at the different scales; see however TN). The shock radius is much closer to the virial one in the external scenario, since the external gas is cold and its infall is not slowed by the pressure support while it is accreted. The largest difference in the shock position are predicted at low masses, where, unfortunately, the shock feature is currently hard to detect due to the low

surface brightness.

Another way to break the degeneracies between the internal and the external scenarios, is to look at the global properties of high redshift halos, for which the expected differences are larger. Indeed, the entropy level is the major driver of the evolution of the global properties of X-ray halos (see also Bower 1997). At large redshifts ($z \geq 1$) the luminosity and temperature evolution depends on the intensity and the timescale of the non-gravitational heating. In the internal case, the luminosity and temperature have a flatter time dependence. The shock radius is always close to the virial radius (third panel) in the internal heating scenario, because the entropy of the external gas is always negligibly small. Thus the epoch and distribution of the heating affects global quantities, such as the contribution of X-ray halos to the X-ray background (see Wu, Fabian & Nulsen 1999, where the gas is heated along the merger tree of halos and requires an average extra energy of 1 – 3 keV per particle). However, we recall again that the many parameters produce a large degeneracy in the internal scenario. The external scenario, instead, provides better defined predictions, since it depends only on the initial value of the entropy. This further strengthens our claim that the best way to probe the thermodynamic history of the ICM is by looking at the entropy profile of nearby halos rather than the global properties of unresolved distant halos.

3. Simulated Observations and Feasibility

Here we focus on the observation of nearby halos. This is the strategy that we propose as the best way to investigate the thermodynamic history of the baryons, taking advantage of the spatial and spectral resolution of present day X-ray missions. In particular the external heating scenario can be tested by the detection of the external entropy level around present day clusters, allowing the accretion shock itself to be located. A power law entropy profile, $K \propto r^{1.1}$, is expected between the shock radius and the transition radius r_t . Within this last radius, a flatter entropy profile will mark the original entropy plateau, partially eroded by cooling.

As described in §2, the two dominant, gravitationally-driven, mechanisms for changing the thermodynamic state of cluster gas are shock heating and adiabatic compression. While shock heating occurs principally at the accretion radius, adiabatic compression will occur both interior and exterior to this radius. As shown above, adiabatic compression of gas during accretion (prior to being shocked) will raise the external gas temperature to values dependent on the initial entropy. The average entropy in the external IGM at $z = 0$ can span an order of magnitude and still give a good fit the L - T relation.

In the case of a constant entropy, the range is $K_* = 0.2 - 0.4 \times 10^{34} \text{ erg g}^{-5/3} \text{ cm}^2$, which corresponds approximately to pre-shock (adiabatically-raised) temperatures of $kT_e \sim 0.1 \text{ keV}$ maximum. Another interesting possibility is to assume a strong evolution in the entropy, of the form $K_* \propto (1+z)^{-2}$. This case gives a good fit to the local L - T , and at the same time has a value as high as $K_*(0) = 3 \times 10^{34} \text{ erg g}^{-5/3} \text{ cm}^2$ in the external gas, corresponding to a temperature of

$\simeq 1$ keV. Despite the very high final value of the entropy, the total (average) energetic budget is less than 0.1 keV per particle, even lower than in the case with constant $K_* \simeq 0.3$. The reason is that in the constant entropy case, most of the energy is released at high redshift, when the density is higher, while if $K_* \propto (1+z)^{-2}$, most of the energetic budget is released only at small z . We also consider this case since from the observational point of view it is one of the most tractable; an external temperature of $\simeq 1$ keV makes the gas (at an overdensity of $\simeq 10$) detectable in emission. We note that such high temperatures in the infalling gas can also be achieved in the case in which the gas is previously gravitationally shocked in filaments (see Cen & Ostriker 1999 and references therein). As we will discuss later, this gravitational contribution to the external entropy may help in attaining a large value of K_* in the outskirts of clusters.

Once the external level of the entropy is assumed, the other relevant piece of information is that the gas density immediately exterior to the shock will be no more than a factor of ~ 4 lower than that at the inner shock boundary, following equation 2.

It is also a consequence of the increasing shock strength at larger radii and of the adiabatic compression that a mildly negative (radially decreasing) temperature gradient is expected, in good agreement with current observations of clusters (Markevitch 1998). The temperature gradients are expected to be stronger when the entropy distribution gets flatter, until the adiabatic limit $T \propto \rho^{2/3}$. For simplicity, in rich clusters we will consider an isothermal distribution of gas within the shock radius, since the predicted temperature profiles can be well approximated as constant (the predicted polytropic index is $\gamma_p \simeq 1.1$, where $\gamma_p = 1$ is the isothermal case, see Figure 2).

What is the best strategy to investigate the described scenarios? Recent X-ray data lack the necessary combination of both spatial and spectral resolution to have routinely detected the accretion shock and detailed entropy profiles of clusters. The same situation applies for low luminosity groups (for $kT < 1$ keV, the luminosity is often defined within a fixed radius of $100 h^{-1}$ kpc, see Ponman et al. 1996). ROSAT for example, while its limiting surface brightness was quite low (a typical background level $\sim 1 \times 10^{-15}$ erg s $^{-1}$ cm $^{-2}$ arcmin $^{-2}$ in the 0.5-2 keV band), had a point spread function width from $\sim 20 - 60$ arcsec and insufficient spectral sensitivity to constrain temperatures to the precisions required. Attempts to push the capabilities of the ASCA X-ray satellite to their limits and observe this accretion shock in archival data of nearby clusters failed, mainly due to the poor ASCA point-spread function (Gendreau & Scharf, private communication).

Current missions should however be well suited to detecting cluster accretion shocks and entropy profiles. Chandra's high spatial resolution ($\sim 1 - 10$ arcsec) may allow details of the spatial structure of a shock region to be investigated. With an effective area of ~ 4600 cm 2 at 1 keV, XMM has approximately 10 times higher throughput than ROSAT, and combined with a $\sim 6 - 15$ arcsec PSF and excellent spectral resolution is ideally suited to this task. XMM can, for example, detect an accretion shock in the nearby Perseus cluster ($z = 0.018$, $L = 2.8 \times 10^{44}$ erg s $^{-1}$ in the 2-10 keV band) with an exposure of the order of 20 ksec. However, in this case, the area to be searched is extremely large compared to the field of view of XMM.

For the lower mass groups the detection, or non-detection, of the accretion shock is much more difficult. However, determining the emission profile beyond the regime currently studied ($\sim 100 h^{-1} \text{kpc}$) and the nature of the entropy profile will be quite feasible. In both cases (rich and poor systems) a key observational criteria will be the ability to detect emission at a level of $\sim 10^{-16} \text{ erg s}^{-1} \text{ cm}^{-2} \text{ arcmin}^{-2}$ (see Figure 2). Additionally, the ability to accumulate sufficient counts to constrain gas temperatures to precisions of 10-20% will be necessary. In general, with a typical background, we find that to measure the gas temperature with a precision of $\sim 10 - 20\%$ requires at least $\sim 1000 - 2000$ source photons respectively for low ($\sim 1 \text{ keV}$) and high ($\sim 8 \text{ keV}$) temperatures. This is a consequence of lower temperature spectra having more photons on the exponential cutoff, where the impact of temperature is strongest.

As an observational baseline for rich clusters we have chosen the Abell 2029 system. At a redshift of $z = 0.0767$ and with $L_{2-10\text{keV}} = 2.07 \times 10^{45} \text{ erg s}^{-1}$ ($h = 0.5$) and $kT = 7.8 \text{ keV}$ (David et al. 1993) this cluster presents an optimal angular scale ($\sim 30 \text{ arcmin}$) and surface brightness. In addition Abell 2029 is a strong cooling flow cluster, and, at least in the inner regions, appears to be in equilibrium with no sign of merging of cluster subunits (Sarazin et al 1998). The core radius of $0.164h^{-1} \text{ Mpc}$, corresponds to $\sim 2.5 \text{ arcmin}$. Assuming $\beta = 2/3$, we obtain an estimated surface brightness at the shock of $\sim 1 \times 10^{-16} \text{ erg s}^{-1} \text{ cm}^{-2} \text{ arcmin}^{-2}$, in close agreement with our model (see Figure 2).

We can now ask what would be required to measure the entropy profile to an emission level of $\sim 10^{-16} \text{ erg s}^{-1} \text{ cm}^{-2} \text{ arcmin}^{-2}$, i.e., to the shock radius. Combining the expected count rates (from XSPEC) for the PN +2MOS for a 7.8 keV plasma and the expected background counts we estimate that to achieve an emission detection of $\sim 6\sigma$, and at least 2000 cluster photons, requires $\sim 70 \text{ ksec}$ and counts accumulated from $\sim 270 \text{ arcmin}^{-2}$. Given the angular dimensions of A2029 we could meet these criteria with 4 XMM pointings of 70 ksec, equally spaced around the expected $\sim 20 \text{ arcmin}$ shock radius. The detection of the accreting gas beyond the shock radius is more difficult, since the surface brightness of the external gas can be an order of magnitude lower. We therefore perform a more realistic simulation in order to assess the feasibility of its detection.

Using QUICKSIM (Snowden 1998) and XSPEC we have simulated a range of XMM observations of cluster gas emission. The simulated cluster (group) is orientated such that the XMM field of view is centred on the shock radius. We simulate both the PN and two MOS EPIC cameras. The internal and cosmic background count rates in the 0.1 – 12 keV band at the coordinates of Abell 2029 are estimated to be $3.67 \times 10^{-3} \text{ ct s}^{-1} \text{ arcmin}^{-2}$ (PN) and 1.11×10^{-3} (MOS) and are included.

We began by simulating a 200 ksec XMM observation of A2029 with a pointing offset $\sim 20 \text{ arcmin}$ from the cluster center (i.e. still within the expected shock radius). The external entropy level is set to $K_{34} = 3(1+z)^{-2}$. The assumed surface brightness profile is the one shown in Figure 2 as a long-dashed line, which is flatter than the average expectation but better resembles the realistic case of A2029. We choose Λ CDM as the background cosmology. A critical universe has

larger accretion rates at $z = 0$, and then smaller shock radius, with respect to the Λ CDM case (in a Λ CDM universe, a shock radius $\simeq 20\%$ larger than the virial one is expected, see TN, and Figure 4). The resulting outputs are spatially and spectrally analyzed with XSELECT and XSPEC, assuming an absorbed Raymond-Smith spectrum. Background counts are subtracted for all spatial data bins using a simulated observation of blank sky, to account for vignetting effects. The spectral fits are performed in concentric annuli, centred on the cluster core. The neutral hydrogen column density is fixed ($N_H = 3 \times 10^{20} \text{ cm}^{-2}$ to match the value at A2029) and the redshift is fixed, while the temperature, normalization and metallicity are allowed to vary. The metallicity is always poorly constrained in these simulations.

The simulated cluster observations are shown in Figure 5, where only the data of the PN detector have been used. In a more realistic observation, the use of the two MOS detectors significantly aids obtaining a stronger signal, or can decrease the required exposure time (see Figure 6). The errors in the figure correspond to 1-sigma. In the first case, the external gas is detected and its temperature measured with about 20% uncertainty (1 sigma). The reason for the small error in the external temperature, despite the low emissivity of the external gas, is due to its value $kT_e \approx 0.7$; for this value the exponential cutoff, from which the temperature is measured, falls in the spectral region of maximum sensitivity for XMM. In the third panel the resulting entropy profile is shown. Despite the large uncertainty in the external value, the discontinuity in the entropy is visible. We point out that we assumed an external density profile $\rho_{ext} \propto r^{-2}$. The presence of substructures, such as small clumps being accreted by the cluster, can make the gas much more visible in emission, due to the enhanced density. Moreover, the entropy of the gas is not changed by the presence of substructure, which contributes only with adiabatic compression. Therefore we believe that the case shown in Figure 5 is to be considered realistic, if not pessimistic.

The second cluster case (Figure 5) envisages a strong shock front with a cold, low-emission external plasma ($kT_e < 0.1 \text{ keV}$), corresponding to the case with $K_{34} \leq 0.3$ constant (here in a Λ CDM; c.f. 2nd row in Figure 2). In this case only the gas internal to the shock radius is detectable, due to the low entropy of the external gas. The non-detection of an external gas halo would not provide any direct constraint on the external entropy level. Note that the region of the cluster being observed here is at a radius approximately twice that of the last significant point of Sarazin et al. (1998): the surface brightness profile in clusters has never been tested to such large radii.

Finally, the third case (Figure 6) is expected to represent lower mass groups: pure adiabatically compressed ICM with a flat entropy profile, and a corresponding steeper temperature gradient following $T \propto \rho^{2/3}$. The emission from the halo smoothly fades into the external IGM, without any discontinuity. In this case, with $K_{34} = 0.3$ (in Λ CDM), the surface brightness is characterized by a relatively large core. A very interesting aspect of this observation is the detection of emission from small groups at an unprecedented distance from the center. At the same redshift of A2029, 6 arcmins correspond to $0.4 h^{-1} \text{ Mpc}$. At such a radius, the surface brightness and the temperature gradient are clearly detected. The entropy profile is flatter than the shocked power law in the center, but the errors are too big at $0.4 h^{-1} \text{ Mpc}$ to discriminate between a shocked and an adiabatic profile

in the very external regions.

As already mentioned, such low surface brightness emission is now emerging from ROSAT data (Helsdon & Ponman 2000) and predicted by TN. We recall that for practical reasons the current luminosities of loose groups are estimated only within a fixed radius of $100h^{-1}$ kpc (see Ponman et al. 1996), while the total luminosities can be higher by a factor larger than 3 when including all the gas accreted from the halo. Note however, that here and in TN we define an *accreted* mass of baryons $M_B = f_B M_{tot}$. In the case with $K_* \geq 0.1$, the most external part of this gas is compressed (but not shocked) by the presence of the potential well and can be located at radii as large as three times the virial radius, thus it can hardly be said “to be accreted”. This reflects the difficulty in defining X-ray emission in small mass halos, in contrast to large mass halos where the X-ray emission is dominated by the central regions. These considerations add further interest to tracing the X-ray emission of small mass objects to the largest radii.

In Figure 6 we show, as a function of the total X-ray luminosity, the exposure times needed with XMM to detect the emission interior and exterior to the accretion shock with a signal to noise of 5, *and* enough photons to derive the temperature to within 20% uncertainty. Here we use the 2 – 10 keV luminosity, and map to T using the 2-10 keV EXOSAT L - T relation (David et al. 1993). We have assumed the same redshift as Abell 2029 ($z = 0.0767$), $\beta \simeq 0.7$, and an external temperature of about 1 keV. As we already discussed, such an external temperature is expected in the case with $K_{34} = 3(1+z)^{-2}$, while a constant $K_{34} \simeq 0.2 - 0.4$ would give an almost undetectable external gas. Thus we use Figure 6 as a guide to the needed exposure time in the cases when the shock is detectable (i.e., $kT > 0.2$ keV); we recall that temperatures lower than 1 keV (but still larger than 0.2 keV) are more easily constrained due to their stronger exponential cutoff. The limits in Figure 6 are derived using the signal in the PN + 2MOS detectors, for different choices of the ratio R_S/R_V of the shock to the virial radius (as long as $\rho_i/\rho_e > 1$). We have always assumed the shock fronts to be at the center of the XMM field of view. The small circle represents our simulated observation of Abell 2029. The constraints on the observation times are dominated by the requirement to have 4000 and 2000 photons respectively inside and outside the shock (continuous lines) while the requirement of the 5-sigma emission detection becomes dominant at lower luminosities (dashed lines). It is clear that, with sufficient exposure at lower luminosities, the shock/adiabatic transition can be mapped to a considerable extent, allowing a direct test of the general picture summarized in §2.

Looking further ahead, two possible missions would make the cluster accretion shock a routine observation in studies of clusters. ESA’s X-ray evolving Universe Spectroscopy (XEUS) mission, has design goals for a 3×10^5 cm² effective area (~ 70 times larger than XMM) and sub 2-arcsec imaging, with high spectral resolution. NASA’s CONSTELLATION-X with a factor 20-100 times larger area than current missions, plus the ability to perform high-resolution spectroscopy of extended objects, could potentially see line emission from pre-shock gas superimposed on the continuum emission of the shocked gas.

4. Discussion

From empirical evidence it seems clear that non-gravitational heating plays a key role in the thermodynamics of the ICM, but the physical mechanism responsible for this heating is not known. A debate exists over whether the sources of heating are mostly stars or AGN (see Wu & Fabian 1999; Valageas & Silk 1999; Menci & Cavaliere 2000; Loewenstein 2000). Numerical simulations that try to include stellar feedback and cooling still have difficulties in linking the small scale physics to the large scale dynamics of the ICM. Our approach starts simply from the analysis of the thermodynamics of the ICM as it is seen in local, and possibly distant clusters, and attempts to answer the most direct questions. We do not build a heating scenario a priori, rather we want to investigate possible scenarios by directly studying the thermodynamic state of the ICM. A key question that we address here is what if the gas has been heated before or after the collapse of the X-ray halo, or, in other terms, at low (with a relatively small energy input) or at large densities (with a larger energy budget)? Here we briefly review the consequences for a scenario where stars provide most of the heating energy.

As described in §1, the entropy level measured in high- z Ly α clouds is low with respect to the level observed in clusters of galaxies. From Figure 10b of Ricotti et al. 2000, we can interpolate $K_{Ly\alpha} \sim 1.6 \cdot 10^{-2} (1+z)^{-1} \times 10^{34} \text{ erg g}^{-5/3} \text{ cm}^2$; higher values of this entropy would make the IGM invisible in absorption. Thus, we estimate that the ratio of the entropy K_{cl} observed in the clusters to that observed in Ly α is $K_{cl}/K_{Ly\alpha} \simeq 10(1+z)$. This difference is even larger for the higher values of K_* that enable a good fit to the local L - T relation and are still allowed by current data.

If we assume that the gas seen in the Ly α clouds is representative of the majority of the IGM, we are witnessing a clear evolution in the equation of state of the diffuse baryons going from the low densities of the Ly α clouds to the higher densities of the X-ray halos. In the framework of the entropy model, this indicates that the IGM undergoes substantial heating just before or after being accreted into the potential wells of groups and clusters. Additionally, the chemical properties of the IGM seen in the Ly α forest are different from those of the ICM in clusters, indicating that the ICM is affected by star formation processes and chemical enrichment, with a commensurate amount of entropy production. The subsequent questions are: when does this heating occur? Can the star formation processes do the job? To determine if star formation processes can be solely responsible for the excess entropy or just provide a minor contribution, a clear correlation between the epoch of star formation and that of the excess entropy production must be established.

From the entropy profiles of local clusters we can extract temporal information. We predict a major feature of these profiles to be the transition between a shock induced power law and a central (adiabatic) entropy core. When the entropy plateau is eroded by cooling, especially in larger halos, the central entropy level can no longer be directly related to the initial K_* value. However, the transition between the shock and the adiabatic regime is still a relevant and robust feature, marked by a change of slope in the entropy profile. Meaningful quantities are this transition radius r_t , and the baryonic mass enclosed within the radius itself, M_{ad} . These two quantities, in the external

heating scenario, are almost constant between clusters and groups, with a clear dependence on the parameter K_* (see Figure 7). The baryonic fraction, of course, refers only to the diffuse, hot gas, and not to gas that may have cooled and sunk to the center. So, as a first approximation, the measure of M_{ad} or r_t at several mass scales will provide a test of the simplest external scenario with a single value for K_* , and at the same time an indication on the level of K_* itself. Moreover, in larger halos, the internal adiabatic core has been accreted at higher redshift (third panel of Figure 7). Detecting the presence of the adiabatic transition in large halos, will put a lower limit to the redshift when the entropy K_* must be already in place.

In the internal case, a transition radius is not defined. Rather, the non-gravitational entropy contribution is simply superimposed on the shocked profile. We do not consider a physical model for the internal heating, and thus we do not make specific prediction for the corresponding entropy profile. Nevertheless, the detection of a break in the entropy profile, together with a constant baryonic mass enclosed within r_t , would favour the external scenario. In this way the measure of M_{ad} and r_t can significantly constrain this model and probe if the stellar populations provide the bulk of the excess entropy. These pieces of information can be combined with other measures from different wavelengths to better evaluate the contribution of star formation processes to the global heating.

The final part of this discussion is devoted to the effect of substructures in the infalling medium. Some of the baryons can be shocked in small sub-halos before being accreted by the main progenitor. Such a gravitationally-produced entropy would raise the average entropy level around large clusters of galaxies, with respect to the average value K_* in the non-shocked gas. However, the entropy which is generated in these gravitational processes does not break the self similarity, since it always scales with the mass of the accreting halo. In other words, shock heating processes such as these are not able to generate an entropy plateau in the center of X-ray halos. Moreover, in the presence of a minimum entropy K_* , such external gravitational contribution rapidly vanishes at small scales, since the satellites of smaller halos are correspondingly smaller and unable to shock the baryons. Thus, the net effect of a moderate amount of substructure around halos is to enhance the detectability of the gas without changing its entropy.

In the present treatment we are not including the *bow shocks* developed through the merging of cluster subunits of comparable mass (indicated by *ASCA* and *ROSAT* observations, cf. Henriksen & Markevitch 1996, Donnelly et al. 1998). In this case strong non-equilibrium features appear (hot spots) and the plasma is vigorously stirred. However, the occurrence of large, violent mergers is expected to be relatively rare in (for example) Cold Dark Matter dominated cosmologies within the framework of the extended Press-Schechter theory. Most of the mass growth of a typical cluster occurs by accretion of small clumps and diffuse matter onto a main progenitor, the relative amounts of which depend on the details of the cosmology and mass power spectrum. In most CDM models, dynamically *quiet* clusters always constitute a significant fraction of the total population, especially at $z = 0$. It is these systems that are most likely to exhibit well defined accretion shocks. The picture is different at redshift $z \simeq 1$, where the accretion rate and then the rate of massive merger

are about an order of magnitude larger with respect to $z = 0$. We estimate (from the extended PS theory) that the average number of major mergers (i.e., with a mass ratio larger than 0.3) occurring within 1 Gyr, is < 0.1 at $z = 0$ and $0.3 - 0.6$ at $z = 1$ in a Λ CDM cosmology. Thus the fraction of X-ray halos possibly affected by massive merger increases dramatically at high redshifts. Such a population of halos would ideally be modelled with hydrodynamical simulations, which can capture the full three dimensional complexity of the processes.

5. Conclusions

In this work we have described how to investigate the thermodynamics of the intra-cluster medium by resolving the entropy distribution within X-ray halos. The ability to spatially and spectrally resolve nearby groups and clusters ($z \leq 0.1$) with current X-ray satellites, can provide many crucial observations: the measure of the entropy level of the non-shocked gas at $z \simeq 0$ around clusters of galaxies; the detection of the extended, low surface brightness emission at large radii in groups, and the transition from the adiabatic to the shock regime imprinted in the inner entropy profile of X-ray halos (expected at about $r_t \simeq 0.2 - 0.4h^{-1}$ Mpc in the external scenario). Such observations will help in probing the two basic scenarios adopted here to describe the non-gravitational heating of the ICM: *external* and *internal*.

In the simpler case of the external scenario, the only free parameter is the entropy excess K_* initially present in the diffuse IGM. In this case, entropy profiles will statistically constrain the value of K_* and can be used to put a lower limit on the redshift of the heating. This will allow an estimation of the epoch and energetics of the heating process itself, and will help to answer the question of whether or not the star formation processes are responsible for the bulk of the entropy excess.

One of the most exciting possibilities is the direct measurement of the external entropy from the emission of the accreting IGM just outside the shock radius of very massive clusters.

In detail, the detection of the external entropy of the pre-shocked gas requires a measurement of both the surface brightness and temperature of cluster gas around the shock radius. With such data, the entropy profile across the shock can be derived, and hence the thermodynamic state of both the ICM *and* the IGM. The detection of accretion shock signatures in rich clusters, together with the observation of constant entropy profiles in groups, would be consistent with the hypothesis of an excess entropy in the external IGM, accreted by dark matter halos. In particular, if the measured entropy level in the gas around clusters and in groups is similar, the simple scenario of homogeneous entropy production in the IGM at high redshifts will be strongly supported. This would simultaneously help constrain physical models for the generation of the entropy.

We describe simulated observations of clusters and groups with XMM to assess feasibility. For two representative values assumed in the external entropy, we show how to detect the low-surface brightness gas at large radii both in large and small halos. In particular, in large halos a

discontinuity in the entropy may be visible, corresponding to the shock radius, while in small halos, a continuous isentropic distribution is expected, possibly extending to very large radii.

A failure to detect the excess entropy in outer, non-shocked gas in massive clusters, would favour the internal scenario, in which the excess entropy is produced within the X-ray halo after the accretion, thus when the gas has already reached higher densities. In this case the energy budget required to attain the same entropy excess at $z = 0$ is much higher (more than 1 keV, with respect to the $\simeq 0.1$ keV required in the external scenario). Moreover, the internal scenario may leave an imprint in the *internal* entropy profile of X-ray halos which is at variance with the profiles $K \propto r^{1.1}$ expected in the external scenario. Indeed, the capabilities of current X-ray satellites may be sufficient to image the structure of enhanced internal entropy production.

Such observations would therefore provide crucial information at the confluence of many different physical processes involving both baryons and dark matter, that put in a common perspective an enormous amount of data, both in the optical and the X-ray band. At present there are no other viable observations which can connect the entropy of the IGM detected, e.g., in the Ly α forest with the entropy level required to explain X-ray constraints from galaxy clusters and groups. We show how an instrument such as XMM can relatively easily perform the necessary measurements and hope this work encourages future observations which will directly test the cluster physics described here.

We thank Megan Donahue and David Strickland for their help in the use of XSELECT and XSPEC. We acknowledge interesting discussion with the participants in the Milano 1999 workshop on “Evolution of Galaxies in Clusters”, especially A. Babul, R. Bower, and N. Menci. We thank also the anonymous referee for stimulating comments. This work has been supported by NASA grants NAG 8-1133. CAS acknowledges the support of NASA grant NAG 5-3257.

REFERENCES

- Allen, S.W., & Fabian, A.C. 1998, astro-ph/9802219
Arnaud, M., & Evrard, A.E. 1999, MNRAS, 305, 631
Balogh, M.L., Babul, A., & Patton, D.R. 1999, MNRAS, 307, 463
Bertschinger, E., 1985, ApJS, 58, 39
Blanchard, A., Valls-Gabaud, D., & Mamon, G.A. 1992, A&A, 264, 365
Borgani, S., Rosati, P., Tozzi, P. & Norman, C. 1999, ApJ, 517, 40
Bower, R. G., 1997, MNRAS, 288, 355
Bryan, G.L., & Norman, M.L. 1998, ApJ, 495, 80
Cavaliere, A., & Fusco Femiano, R., 1976, A& A, 49, 137

- Cavaliere A., Menci N., Tozzi P., 1997, ApJ, 484, L21
- Cavaliere A., Menci N., Tozzi P., 1999, MNRAS, 308, 599
- Cen, R., & Ostriker, J. P. 1999, ApJ, 514, 1
- Dahlem, M. (Editor) et al. 1999, “The XMM Handbook”, http://astro.estec.esa.nl/XMM/user/uhb/xmm_uhb.htm
- David, L. P. et al, 1993, ApJ, 412, 479
- Donnelly, R. H., Markevitch, M., Forman, W., Jones, C., Churazov, E., & Gilfanov, M. 1998, ApJ, 500, 138
- Ettori, S. 2000, MNRAS, 311, 313
- Evrard, A. E., 1990, ApJ, 363, 349
- Evrard, A. E., & Henry, J. P. 1991, ApJ, 383, 95
- Evrard A. E., Metzler C. A., & Navarro J. F., 1996, ApJ, 469, 494
- Hellstein, U., Gnedin, N.Y., & Miralda–Escudé, J. 1998, ApJ, 509, 56
- Helsdon, S.F., & Ponman, T.J. 2000, MNRAS, 315, 356
- Henriksen, M. J., & Markevitch, M., 1996, ApJ, 466, L79
- Henry J. P. 1997, ApJ 489, L1
- Henry J. P. 2000, ApJ, 534, 565
- Kaiser, N. 1991, ApJ, 383, 104
- Knight, P. A., & Ponman, T. J. 1997, MNRAS, 289, 955
- Lacey, C., & Cole, S. 1993, MNRAS, 262, 627
- Landau, L. D., Lifshitz E. M. 1959, *Fluid Mechanics* (London, Pergamon press), p. 329
- Lewis, G.F., Babul, A., Katz, N., Quinn, T., Hernquist, L. & Weinberg, D. 1999, preprint, astro-ph/9907097
- Lieu, R., Bonamente, M., & Mittaz, J. 2000, preprint, astro-ph/0001127
- Lloyd–Davies, E.J., Ponman, T.J., & Cannon, D.B. 2000, MNRAS, 315, 689
- Loewenstein, M. 2000, ApJ, 532, 17
- Markevitch, M. 1998 ApJ, 504, 27
- Menci, N., & Cavaliere, A. 2000, MNRAS, 311, 50
- Metzler, C. A., & Evrard, A. E. 1994, ApJ, 437, 564
- Mushotzky, R. F., & Scharf, C. A., 1997, ApJ, 482, 13
- Ponman, T. J., Bourner, P. D. J., Ebeling, H., & Böhringer, H. 1996, MNRAS, 283, 690
- Ponman, T. J., Cannon, D. B., Navarro, F.J. 1999, Nature, 397, 135 (PCN)
- Renzini, A. 1997, ApJ, 488, 35

- Renzini, A. 1999, Proceedings of the ESO workshop held at Garching, Germany, 14-16 Oct 1998, Jeremy R. Wals, Michael R. Rosa (eds.); Berlin; New York; Springer, p. 185
- Ricotti, M., Gnedin, N. Y., & Shull, J. M. 2000, *ApJ*, 534, 41
- Roettiger, K., Burns, J., & Loken, C. 1993, *ApJ*, 407, L53
- Rosati, P., Della Ceca, R., Norman, C., Giacconi, R. 1998, *ApJ* 492, L21
- Sarazin, C. L., Wise, M. W., Markevitch, M. L., 1998, *ApJ*, 498, 606
- Schaye, J., Theuns, T., Leonard, A., & Efstathiou, G. 1999, *MNRAS*, 310, 57
- Snowden, S. 1999, QUICKSIM Version 1.0.3a, <http://heasarc.gsfc.nasa.gov/docs/frames/xmm-prop-tools.html>
- Strickland, D.K., & Stevens, I.R. 2000, *MNRAS*, 314, 511
- Takizawa, M., & Mineshige, S. 1998, *ApJ*, 499, 82
- Tozzi, P., & Norman, C. 1999, Proceedings of the ESO Symposium held at Antofagasta, Chile, 1-4 March 1999, Jacqueline Bergeron, Alvio Renzini (eds.), Berlin, New York, Springer, p. 180
- Tozzi, P., & Norman, C. 2000, *ApJ* submitted, astro-ph/0003289
- Valageas, P., & Silk, J. 1999, *A&A*, 350, 725
- White, S.D.M., & Rees, M. 1978, *MNRAS*, 183, 341
- White, S.D.M., Navarro, J.F., Frenk, C.S., & Evrard, A.E. 1993, *Nature*, 366, 429
- Wu, K. K. S., Fabian, A. C., & Nulsen, P. E. J. 1999, *MNRAS* submitted, astro-ph/9907112
- Wu, K. K. S., Fabian, A. C., & Nulsen, P. E. J. 1999, *MNRAS* submitted, astro-ph/9910122
- Xue, Y.J., & Wu, X. P. 2000, *ApJ* accepted, astro-ph/0002446

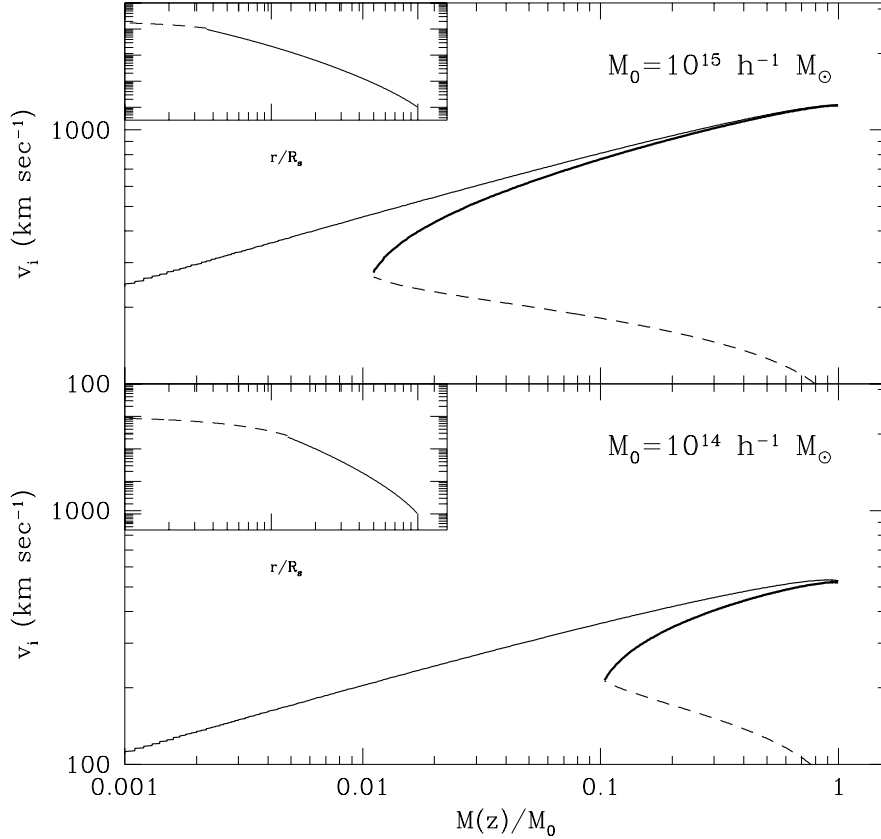


Fig. 1.— The infall velocity at the shock radius of each accreted gas shell as a function of the virialized mass. Here we assumed $K = 0.3 \times 10^{34} \text{ erg cm}^2 \text{ g}^{-5/3}$ in a low density ($\Omega_0 = 0.3$) flat cosmology, for a final mass at $z = 0$ of $10^{15} h^{-1} M_\odot$ (upper panel) and $10^{14} h^{-1} M_\odot$ (lower panel). The straight line is the free fall velocity $v_i \simeq M^{1/3}$, while the thick line is the infall velocity of the baryons, and the dashed line is the sound speed c_s . When $v_i < c_s$ the accretion process is entirely adiabatic, and the accreted gas forms an adiabatic core (dashed line) in the density profiles shown in the inset boxes (for simplicity cooling is not included in the calculation of these profiles).

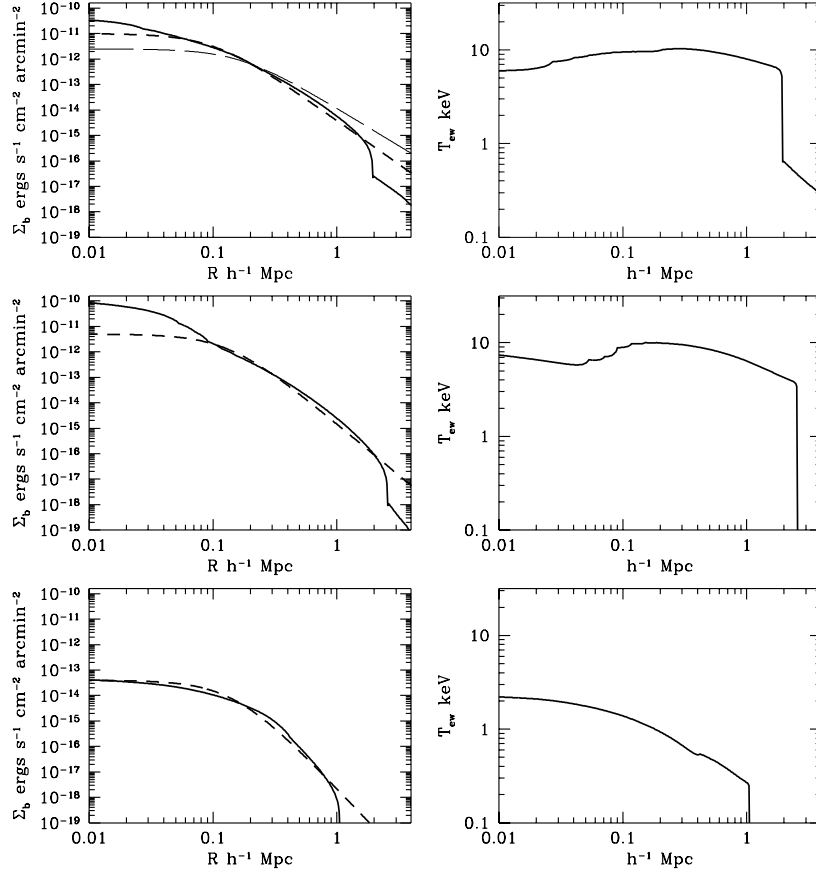


Fig. 2.— Surface brightness and projected temperature profiles extended out of the shock radius for three relevant cases in the external scenario (the entropy and cosmologies have been chosen to emulate the required properties). Top panels: $M = 1.4 h^{-1} 10^{15} M_{\odot}$, tCDM, $K_* = 3(1+z)^{-2}$; middle panels: $M = 1.4 h^{-1} 10^{15} M_{\odot}$, Λ CDM, $K_* = 0.3$; lower panels: $M = 5 h^{-1} 10^{13} M_{\odot}$, Λ CDM, $K_* = 0.3$. The corresponding fits with a beta model are shown with a short dashed line. In the first panel, the long dashed line shows the beta profile used in the simulated observations (§3). In this calculation of the predicted surface brightness the cooling is included (see TN).

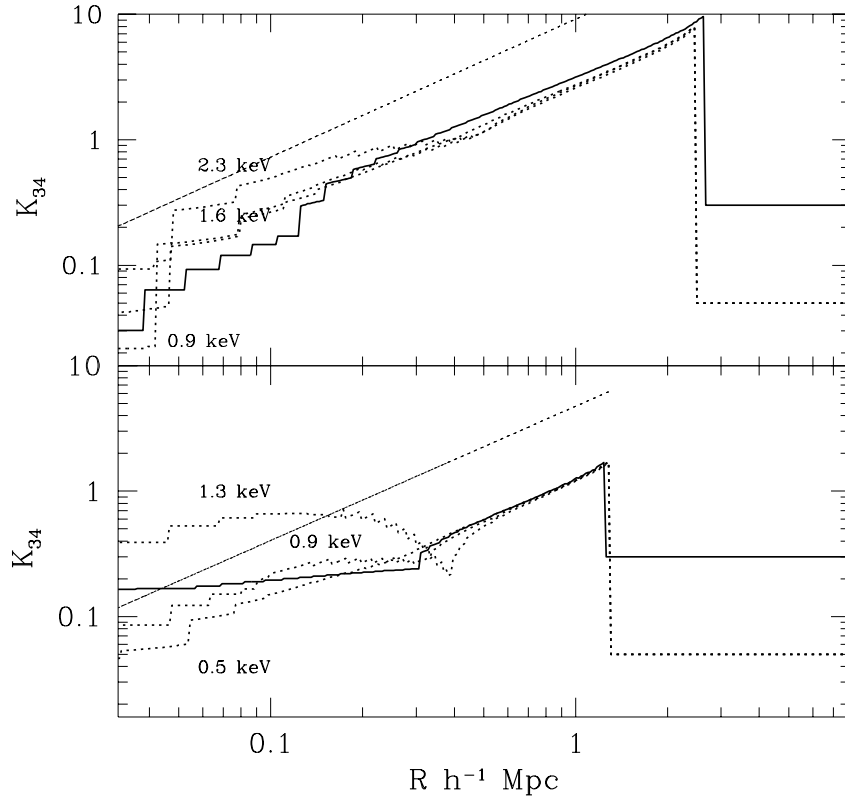


Fig. 3.— The entropy profiles in the external (continuous lines) and the internal (dotted lines) scenario for a rich cluster ($M = 10^{15} h^{-1} M_{\odot}$, upper panel) and a small cluster ($M = 10^{14} h^{-1} M_{\odot}$, lower panel). The entropy level is $K_{34} = 0.3$ in the external scenario. The internal scenario a total budget of 0.5 – 2 keV is released, as shown by the labels. The dashed line is the reference power law of 1.1.

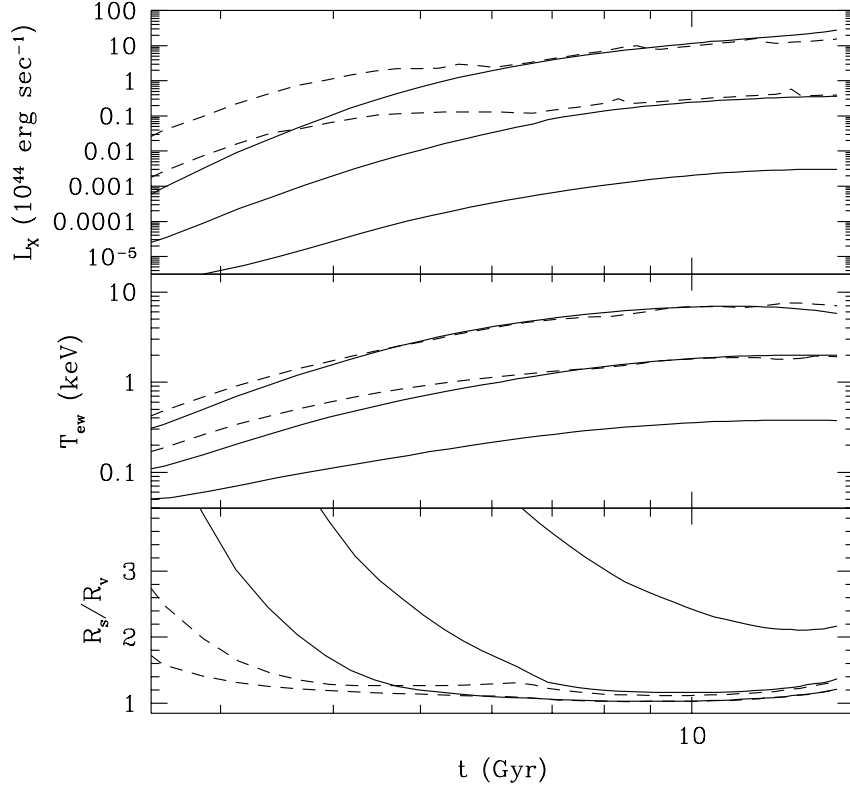


Fig. 4.— Evolution of luminosity, temperature and shock radius for halos of $M = 10^{15} - 10^{14} - 10^{13} h^{-1} M_{\odot}$ (from top to bottom). The external scenario with $K_{34} = 0.3$ is shown as a continuous line, the internal (with an energy budget of 0.9 keV) with dashed lines. A Λ CDM cosmology has been adopted.

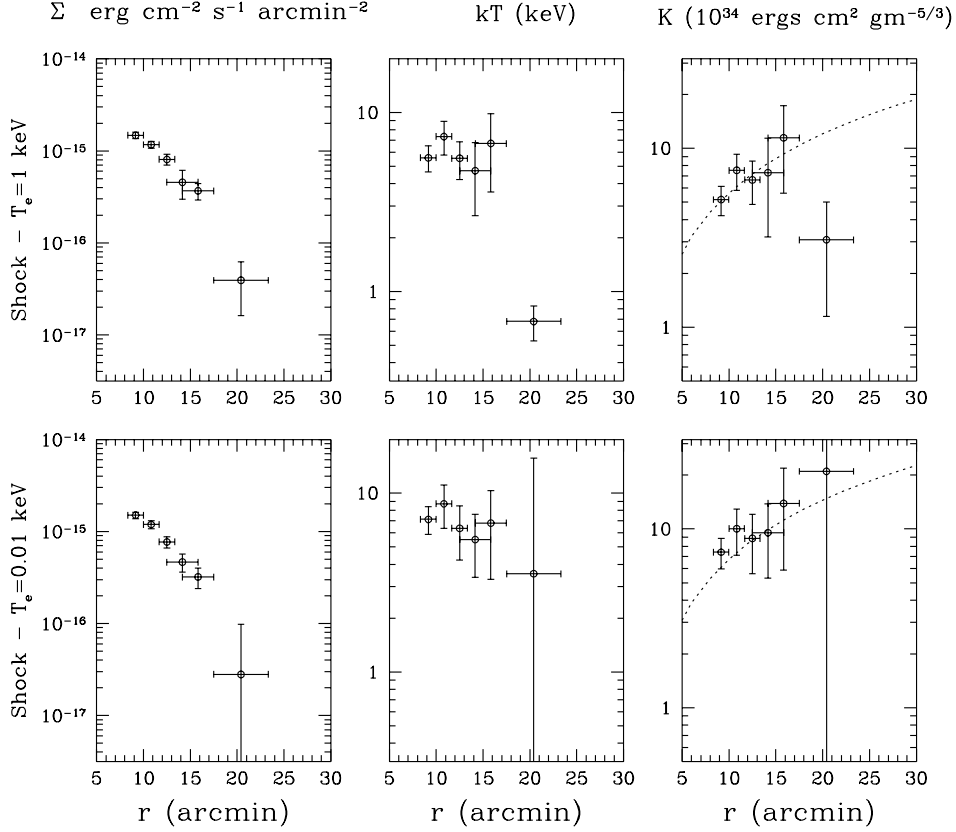


Fig. 5.— Simulated observations based on Abell 209 for the two cases discussed in the text. The three columns show the observed surface brightness, temperature and entropy profiles, with relative error bars (90 % confidence level). A beta-model with $\beta \simeq 0.7$, normalized to the results of Sarazin et al. (1998), has been used. First row: strong shock with an external warm gas ($kT_e = 1$); second row: strong shock with an external cold gas ($kT_e = 0.01$). The dotted line is the power law $r^{1.1}$ predicted for the shocked gas interior to the shock radius.

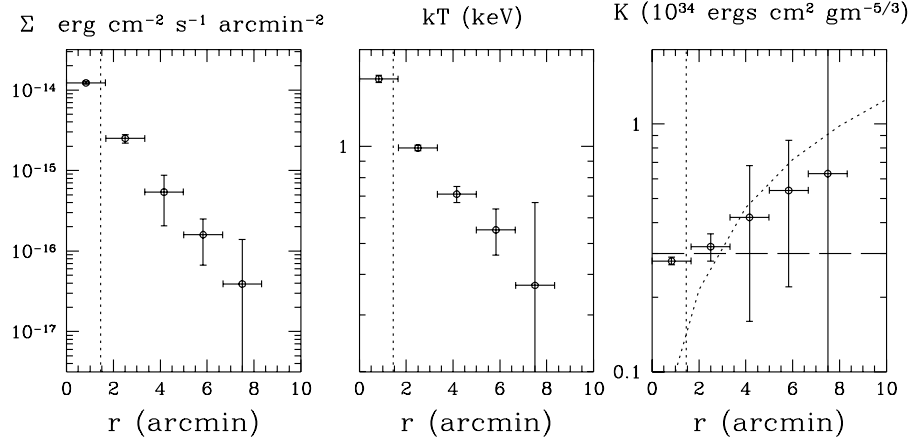


Fig. 6.— Simulated observation of a low mass group at the redshift of A2029, exhibiting an adiabatic profile with no shocks. Note change in x-axis scale from Figure 5. Vertical lines indicate the $100 h^{-1} \text{ kpc}$ scale of current group luminosity measurements. In panel 3 a horizontal line is drawn at the constant (external) entropy level of $K_{34} = 0.3$. Although the entropy is poorly constrained at large radii an inner entropy core is clearly observed ($r < 3 \text{ arcmin}$) and the outer entropy is consistent with these values.

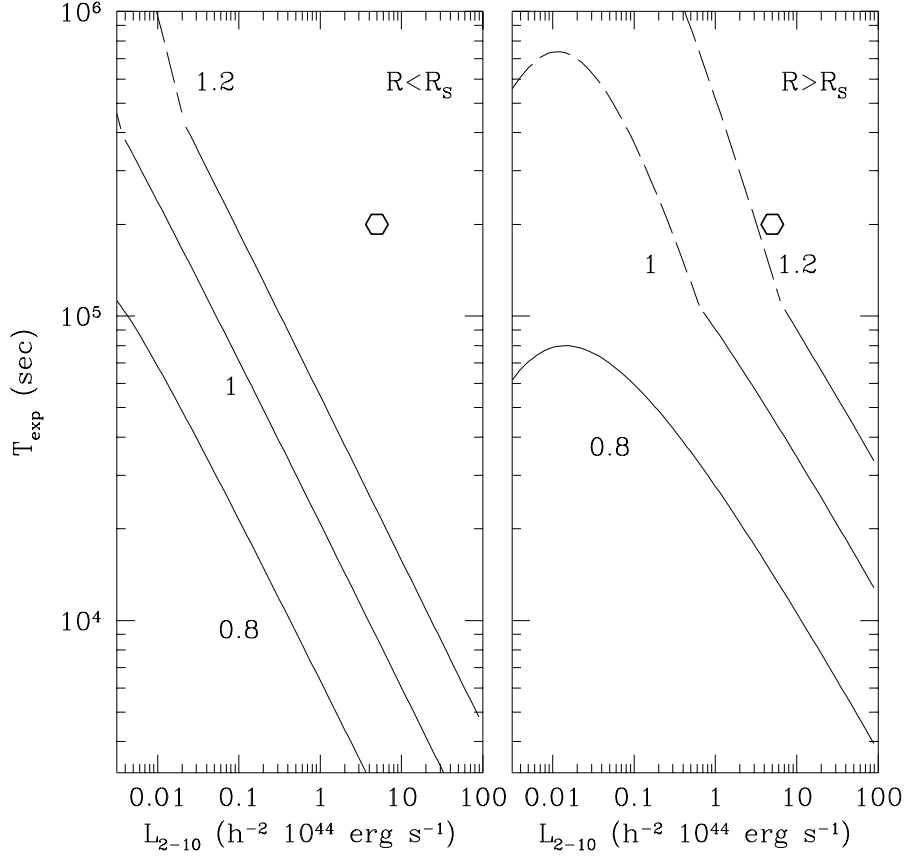


Fig. 7.— The exposure times needed to detect the emission internal (left panel) and external (right panel) to the shock, with a $S/N=5$, as a function of the total 2 – 10 keV luminosity for objects at the same redshift of Abell 2029 ($z = 0.0767$). Here $\beta = 2/3$ and $kT_e = 1$ keV. The limits are derived using the signal in the PN+2MOS detectors (thin filter). Different curves refer to different value of the ratio R_S/R_V . The circle refers to the simulated observations for Abell 2029.

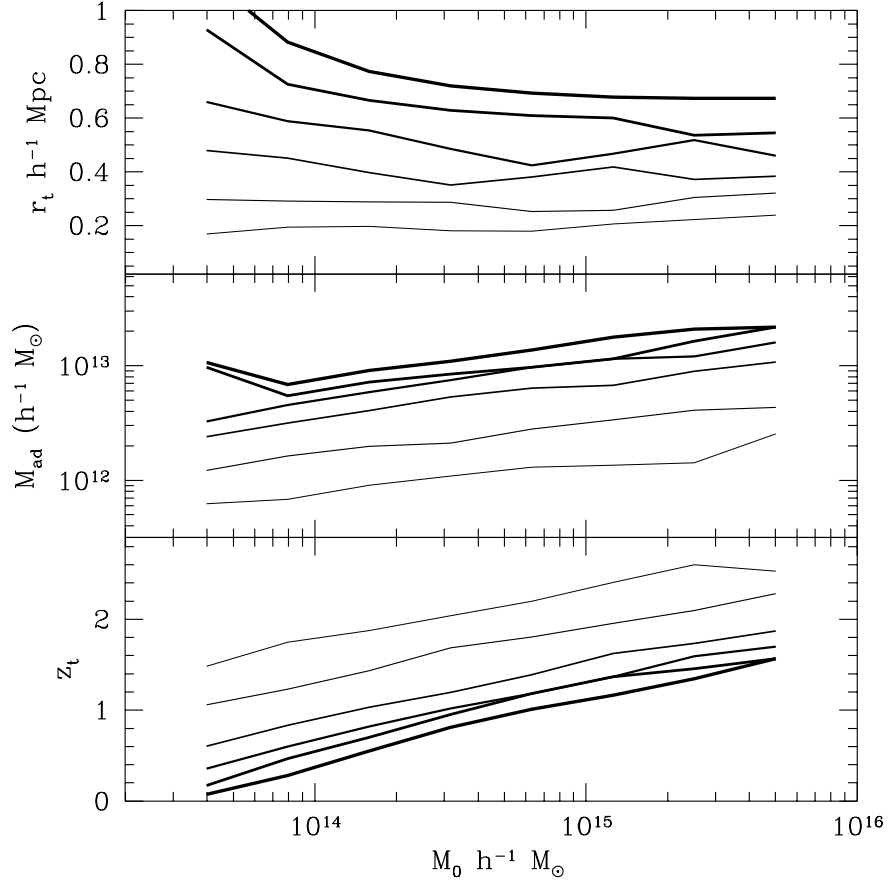


Fig. 8.— The transition radius, the mass included in the transition radius, and the epoch of the adiabatic/shock transition as a function of the total mass scale for the external scenario. The curves correspond to different values of K_* , from heaviest lines to lightest: 0.5, 0.4, 0.3, 0.2, 0.1, and $0.05 \times 10^{34} \text{ erg cm}^2 \text{ g}^{-5/3}$. A Λ CDM cosmology has been adopted.